Metal Complexes of the Schiff Base Derived from Amino Acid and Salicylaldehyde: Synthesis, Characterization, Bioactivities and Molecular Docking Studies

Md. Nur Amin Bitu,[1] Md. Faruk Hossen,[1] Md. Ali Asraf,[1] Md. Masuqul Haque,[1] Ranjan Kumar Mohapatra,[2]
Aly Abdou,[3] Md. Kudrat-E-Zahan[1,*]

[1] Department of chemistry, Rajshahi University, Rajshahi 6205, Bangladesh

[2] Department of Chemistry, Government College of Engineering, Keonjhar, Odisha, India

[3] Chemistry Department, Faculty of Science, Sohag University, Sohag 82524, Egypt

* Corresponding author's e-mail address: kudrat.chem@ru.ac.bd

Abstract: A Schiff base ligand, [3-((2-hydroxybenzylidene)amino)benzoic acid], [$C_{14}H_{11}NO_3$] has been synthesized from the condensation of 3-amino benzoic acid with salicylaldehyde. Also, the ligand was coordinated with Cu(II), Ni(II), Cr(III), Cd(II), Mn(II), Co(II) and Zn(II) metal ions to form their corresponding complexes. The ligand and all the metal complexes were isolated from the reaction in solid form and characterized by elemental analysis, molar conductance, magnetic susceptibility measurements, electronic spectral measurements, IR spectra, ESI-MS spectra, TGA and some physicochemical studies. All the reactions monitored by TLC and UV-visible spectroscopic measurements. The molar conductance values (5–21 S cm^2 mol^{-1}) indicated all the complexes to be non-electrolytic in nature except Cr(III) complex (87 S cm^2 mol^{-1}) which behaves as 1 : 1 electrolyte. Spectroscopic evidence indicated that the Schiff base behaved as N, O donor chelating agents. Magnetic susceptibility value coupled with electronic spectral data suggested that Cu(II), Cd(II), Co(II) and Zn(II) complexes have tetrahedral geometry while Ni(II), Cr(III), and Mn(II) complexes have octahedral geometry. Thermal analysis (TGA and DTG) data showed the possible degradation pathway of the complexes and indicated that the complexes were thermally stable up to (200–300) °C. The quantum chemical features of the prepared ligand and its corresponding metal complexes were computed, and its electronic and molecular structure was refined theoretically. Furthermore, the in silico binding mode of prepared ligand and its corresponding metal complexes with *Escherichia coli* (KAS I-PDB ID-1FJ4) was performed using molecular docking. The Schiff base and its metal complexes have been screened for their antibacterial activity against *Bacillus cereus* and *Escherichia coli*. Among all the synthesized species Cu(II), Cd(II) and Zn(II) complexes were more potential towards the tested pathogens. The cytotoxic activity of Cu(II), Cd(II) and Zn(II) complexes was experimented on human umbilical vein endothelial cells (HUVECs). Among these complexes, Cu(II) complex is found to show higher toxicities than the others on HUVECs.

Keywords: Schiff base, 3-amino benzoic acid, salicylaldehyde, metal complexes, thermal analysis (TGA/DTG), antibacterial activity, cytotoxic activity, HUVECs, DFT calculation, molecular docking.

INTRODUCTION

SCHIFF bases are the condensation products of primary amines and carbonyl compounds. The common structural feature of these compounds is the presence of the azomethine (−HC=N−) group, termed as imines or azomethines.[1] From the past few decades, Schiff bases are playing an important role in the development of coordination chemistry. Schiff base and their metal complexes have been studied extensively due to the relative easiness of preparation, attractive chemical, physical and biological properties[2,3] attributed to the presence of azomethine (−HC=N−) group. Since the azomethine group is responsible for the broad spectrum of biological activities in these compounds, they are used as antimicrobial,[4–6] anti-inflammatory,[7–9] analgesic,[7–10] antitubercular,[11] anticancer,[12,13] antioxidant,[14,15] agents, and so on. The azomethine nitrogen atom may interfere in regular cell functions by forming a hydrogen bond with the active centers of constituent cells.[5,6]

Amino acids, a significant class of organic compounds may take part to synthesis Schiff base by condensation of amine group (NH_2) with any carbonyl compound. They contain potential donor sites such as COOH and NH_2, which have excellent potentiality to coordinate with the metal ions.[16] The Schiff bases derived from amino acids, form stable complexes with transition metals and can act as antimicrobial agent after complexation.[17] Based on the above facts, there exists large interests in the synthesis of amino acid derived Schiff base ligands and their metal complexes due to their biological importance as well as anti-tumor activities.[18] Also, Schiff bases derived from hydroxyaryl aldehydes such as salicylaldehyde shows potential antimicrobial properties.[19,20] A. Blagus *et al.* reported a review article on the structural features of hydroxyaryl aldehydes derived Schiff base.[21] DFT and molecular docking studies of a series of Schiff base ligands derived from salicylaldehyde as potential antibacterial agents was reported by M.I. Ali et al.[22] They studied the in vitro antibacterial activities of the compounds against four bacterial strains *Streptococcus agalactiae*, *Staphylococcus aureus*, *Escherichia coli*, and *Shigella sonnei* by disc diffusion method. All of the synthesized compounds possess to have excellent antibacterial activity.

In this manuscript, we have studied the synthesis and spectral characterization with thermal, antibacterial and cytotoxic properties, DFT calculation and molecular docking of the Cu(II), Ni(II), Cr(III), Cd(II), Mn(II), Co(II) and Zn(II) complexes of 3-amino benzoic acid and salicylaldehyde derived Schiff base.

EXPERIMENTAL

Materials and Methods

REAGENTS AND CHEMICALS
All the reagents used were of analytical grade or chemically pure grade. Solvents were purified according to standard procedures. All metal salts were used as nitrate, chloride or sulphate. Absolute ethanol was purchased from Carew and Co. (Bangladesh) Ltd, dimethyl sulfoxide (DMSO) was purchased from Merck (Germany), diethyl ether, dichloromethane (DCM) and all the metal salts were purchased from BDH (England), dimethylformamide (DMF), iso-propyl alcohol (IPA), 3-amino benzoic acid, salicylaldehyde, potassium hydroxide and anhydrous calcium chloride was purchased from Sigma-Aldrich (USA). Nutrient agar and Dulbecco's modified Eagle medium (DMEM) used as the medium of bacterial growth and cell culture respectively was purchased from thermo-fisher scientific.

PHYSICAL MEASUREMENTS
The melting point of the synthesized ligand and all the metal complexes were recorded in an electro thermal melting point apparatus model No.AZ6512. The electrical conductance of 1.0×10^{-3} mol dm^{-3} solutions of the complexes in DMSO were measured at room temperature using a WPA CM 35 conductivity meter and a dip-cell with platinized electrode. Magnetic moment of the complexes was measured by a SHERWOOD SCIENTIFIC Magnetic Susceptibility Balance (MSB) following the Gouy method. Infrared spectra were recorded as KBr disc in a SIMADZU FTIR-8400 (Japan) infrared spectrophotometer within 4000–250 cm^{-1} range. The electronic spectra of the complexes in 1×10^{-5} M DMSO solution was recorded on SHIMUDZU Spectrophotometer (Model UV-1800). ESI-MS spectra were recorded with an Agilent Technologies MSD SL Trap mass spectrometer with ESI source coupled with an 1100 Series HPLC system for the confirmation of molecular formulas of compounds. Thermogravimetric analysis (TGA) was carried out on Perkin Elmer Simultaneous Thermal Analyzer, STA-8000. Carbon, hydrogen and nitrogen analyses for the complexes were done by Perkin Elmer 2400 organic elemental analyzer-II.

Synthesis Procedures

SYNTHESIS OF SCHIFF BASE LIGAND (L)
The ligand was synthesized by reacting equimolar quantities of salicylaldehyde and 3-amino benzoic acid. For this reaction salicylaldehyde (25 mmol, 2.62 mL) in ethanol (10 mL) was added drop wise to a constant stirring solution of 3-amino benzoic acid (25 mmol, 3.4285 g) in ethanol (20 mL). The mixture was refluxed for 3 hours at 80 °C. During this time, the color of the solution (blood red) turned into yellow. The completion of reaction was
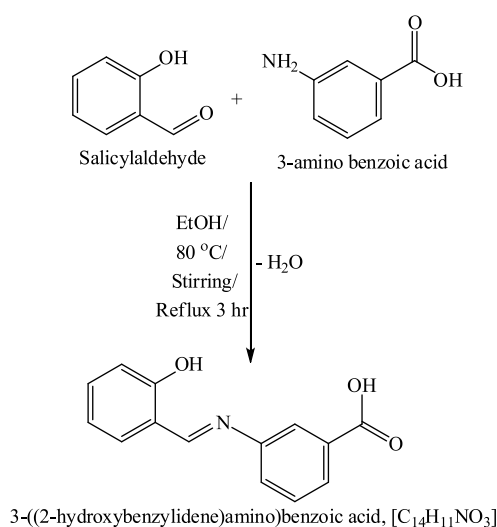
Scheme 1. Synthesis pathway of Schiff base ligand.

monitored using TLC and UV-visible spectroscopic measurement. After completion of the reaction, the volume of the reaction mixture was reduced to half by rotary evaporator. On cooling, a solid product formed. The solid residue was filtered, washed with ethanol, then with diethyl ether several times, and dried in vacuum over anhydrous $CaCl_2$.

The Synthesis pathway of Ligand (L) exhibited in Scheme 1.

Color: yellow, Melting point: 170-171 °C, Yield: 5.1300 g (85 %), FTIR spectral peak (ν / cm^{-1}): 3436 (O–H), 1623 (C=N), 1573 ν_{asy}(COO$^-$), 1418 ν_{sy}(COO$^-$), 1157 (C–O), UV-vis. spectral peak (λ_{max} / nm): 275, 380. Elemental analysis for [$C_{14}H_{11}NO_3$]: M.W. 241.24 g mol^{-1}; Calculated (%): C, 69.70; H, 4.60; N, 5.81. Found (%): C, 68.52; H, 4.46; N, 5.79.

GENERAL METHOD FOR THE SYNTHESIS OF METAL COMPLEXES

The synthesized Schiff base ligand and metal salts were reacted in (1 : 1) molar ratio in order to form the series of metal complexes. To a magnetically stirred suspension of Schiff base ligand $C_{14}H_{11}NO_3$ (1 mmol, 0.4212 g) in ethanol (10 mL) was added equimolar KOH (1 mmol, 0.056 g). The mixture was stirred for half an hour. Then warm ethanolic solution (10 mL) of the corresponding metal salt (1 mmol) as nitrate/sulphate/chloride was added drop wise in this mixture and refluxed for 1 hour. The completion of reaction was monitored using TLC and UV-Visible spectroscopic measurement. The reaction mixture was reduced to half of its volume by evaporation of the solvent in rotary evaporator. The obtained solution was filtered, washed with ethanol then with diethyl ether and dried in vacuum over anhydrous $CaCl_2$. The solid products were found to be soluble in DMF and DMSO and insoluble in water, ethanol, IPA, DCM and diethyl ether.
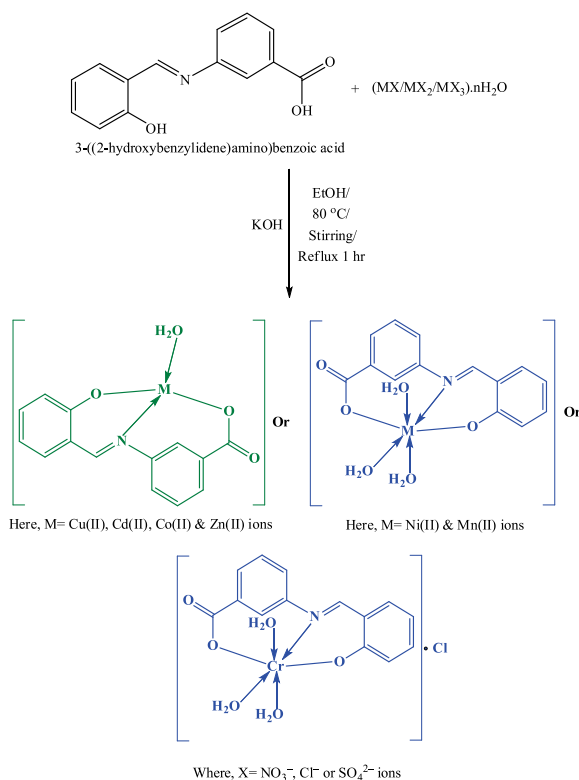
The synthesis pathway of complexes is shown in Scheme 2.

Cu(II) complex (C-1), [Cu($C_{14}H_9NO_3$)·H_2O]
Color: light green, Melting point: 282–283 °C, Yield: 0.4313 g (77 %), Molar conductance (Λ_m / Ω^{-1} cm^2 mol^{-1}) : 6, Magnetic moment (μ_{eff}/B.M.): 1.74, FTIR spectral peak (ν / cm^{-1}): 3435 (O–H)/H_2O, 1616 (C=N), 1544 ν_{asy}(COO$^-$), 1384 ν_{sy}(COO$^-$), 1151 (C–O), 525 (Cu–O), 385 (Cu–N), UV-vis. spectral peak (λ_{max} / nm): 271, 287, 357. Elemental analysis for [Cu($C_{14}H_9NO_3$)·H_2O]: M.W. 320.79 g mol^{-1}; Calculated (%): C, 52.42; H, 3.46; N, 4.37. Found (%): C, 51.47; H, 3.41; N, 4.29.

Ni(II) complex (C-2), [Ni($C_{14}H_9NO_3$) ($H_2O)_3$]
Color: light lemon, Melting point: > 300 °C, Yield: 0.4609 g (75 %), Molar conductance (Λ_m / Ω^{-1} cm^2 mol^{-1}): 20,

Scheme 2. Synthesis pathway of Schiff base metal complexes.

Magnetic moment (μ_{eff} /B.M.): 3.12, FTIR spectral peak (ν / cm^{-1}): 3430 (O–H) / H_2O, 1620 (C=N), 1562 ν_{asy}(COO$^-$), 1384 ν_{sy}(COO$^-$), 1153 (C–O), 529 (Ni–O), 440 (Ni–N), UV-vis. spectral peak (λ_{max} / nm): 257, 381, 575. Elemental analysis for [Ni($C_{14}H_9NO_3$) ($H_2O)_3$]: M.W. 351.97 g mol^{-1}; Calculated (%): C, 47.77; H, 4.30; N, 3.98. Found (%): C, 47.12; H, 4.16; N, 3.76.

Cr(III) complex (C-3), [Cr($C_{14}H_9NO_3$) ($H_2O)_3$]Cl
Color: light brown, Melting point: > 300 °C, Yield: 0.4340 g (72 %), Molar conductance (Λ_m / Ω^{-1} cm^2 mol^{-1}): 87, Magnetic moment (μ_{eff} /B.M.): 3.84, FTIR spectral peak (ν / cm^{-1}): 3429 (O–H) / H_2O, 1617 (C=N), 1561 ν_{asy}(COO$^-$), 1384 ν_{sy}(COO$^-$), 1151 (C–O), 532 (Cr–O), 447 (Cr–N), UV-vis. spectral peak (λ_{max} / nm): 256, 350, 622. Elemental analysis for [Cr($C_{14}H_9NO_3$) ($H_2O)_3$]Cl: M.W. 380.72 g mol^{-1}; Calculated (%): C, 44.17; H, 3.97; N, 3.68. Found (%): C, 44.37; H, 3.88; N, 3.59.

Cd(II) complex (C-4), [Cd($C_{14}H_9NO_3$)·H_2O]
Color: pale yellow, Melting point: 205–206 °C, Yield: 0.4453 g (69%), Molar conductance (Λ_m/ Ω^{-1}cm^{2}mol^{-1}): 5, Magnetic moment (μ_{eff} /B.M.): 0.62, FTIR spectral peak (ν/cm^{-1}): 3428 (O-H)/H_2O, 1619 ν(C=N), 1556 ν_{asy}(COO$^-$), 1384 ν_{sy}(COO$^-$), 1150 (C-O), 526 (Cd-O), 419 (Cd-N), UV-vis. spectral peak (λ_{max}/nm): 274, 339. Elemental analysis for

[Cd(C$_{14}$H$_9$NO$_3$) ·H$_2$O]: M.W. 369.65 g/mol; Calculated (%): C, 45.49; H, 3.00; N, 3.79. Found (%): C, 44.63; H, 3.12; N, 3.58.

Mn(II) complex (C-5), [Mn(C$_{14}$H$_9$NO$_3$) (H$_2$O)$_3$]

Color: light orange, Melting point: 175–176 °C, Yield: 0.4438 g (73 %), Molar conductance (Λ_m / Ω^{-1} cm^2 mol^{-1}): 21, Magnetic moment (μ_{eff} / B.M.): 5.96, FTIR spectral peak (ν / cm^{-1}): 3410 (O–H) / H$_2$O, 1620 (C=N), 1569 ν_{asy}(COO$^-$), 1398 ν_{sy}(COO$^-$), 1156 (C–O), 529 (Mn–O), 439 (Mn–N), UV-vis. spectral peak (λ_{max} / nm): 261, 274, 344, 646. Elemental analysis for [Mn(C$_{14}$H$_9$NO$_3$) (H$_2$O)$_3$]: M.W. 348.21 g mol^{-1}; Calculated (%): C, 48.29; H, 4.34; N, 4.02. Found (%): C, 47.65; H, 4.09; N, 3.94.

Co(II) complex (C-6), [Co(C$_{14}$H$_9$NO$_3$) ·H$_2$O] ·H$_2$O

Color: brown, Melting point: > 300 °C, Yield: 0.4610 g (79 %), Molar conductance (Λ_m / Ω^{-1} cm^2 mol^{-1}): 16, Magnetic moment (μ_{eff} / B.M.): 5.39, FTIR spectral peak (ν / cm^{-1}): 3432 (O–H) / H$_2$O, 1617 (C=N), 1560 ν_{asy}(COO$^-$), 1385 ν_{sy}(COO$^-$), 1148 (C–O), 527 (Co–O), 442 (Co–N), UV-vis. spectral peak (λ_{max} / nm): 262, 283, 380. Elemental analysis for [Co(C$_{14}$H$_9$NO$_3$) ·H$_2$O] ·H$_2$O: M.W. 334.19 g mol^{-1}; Calculated (%): C, 50.32; H, 3.92; N, 4.19. Found (%): C, 49.22; H, 3.94; N, 4.07.

Zn(II) complex (C-7), [Zn(C$_{14}$H$_9$NO$_3$) ·H$_2$O]

Color: off white, Melting point: 175–176 °C, Yield: 0.4281 g (76 %), Molar conductance (Λ_m / Ω^{-1} cm^2 mol^{-1}): 7, Magnetic moment (μ_{eff} / B.M.): 0.60, FTIR spectral peak (ν / cm^{-1}): 3401 (O–H) / H$_2$O, 1617 (C=N), 1565 ν_{asy}(COO$^-$), 1394 ν_{sy}(COO$^-$), 1140 (C–O), 528 (Zn–O), 396 (Zn–N), UV-vis. spectral peak (λ_{max} / nm): 262, 289, 396. Elemental analysis for [Zn(C$_{14}$H$_9$NO$_3$)·H$_2$O]: M.W. 322.62 g mol^{-1}; Calculated (%): C, 52.12; H, 3.44; N, 4.34. Found (%): C, 50.98; H, 3.48; N, 4.23.

DFT Calculation

The prepared ligand and its corresponding metal complexes were optimized using B3LYP method[23–25] with 6-311G(d, p)[26,27] basis set for C, H, N, S, and O atoms and a LANL2DZ[28,29] basis set for metal atoms. The frontier molecular orbitals; Highest Occupied Molecular Orbital (HOMO) and Lowest Unoccupied Molecular Orbital (LUMO) were obtained. The HOMO, LUMO, ionization potential (IP), electron affinity (EA), energy gap (ΔE), chemical hardness (η), and softness (σ) of the investigated compounds were evaluated using the reported equations in literature.[30,31]

Molecular Docking

Molecular docking studies were used to investigate the key interactions of the prepared ligand and its corresponding metal complexes with *E. coli* (KAS I-PDB ID-1FJ4) receptor.[32] The selected protein for docking, *E. coli* β-ketoacyl-acyl carrier protein synthase I (KAS I), is a crucial enzyme involved in bacterial fatty acid biosynthesis. This enzyme, encoded by the fabB gene in *E. coli*, plays a central role in elongating fatty acid chains by catalyzing the condensation reaction between acyl-ACP (acyl carrier protein) and malonyl-ACP, thus extending the carbon chain by two carbons. The crystal structure of *E. coli* KAS I, represented by PDB ID 1FJ4, provides valuable insights into its three-dimensional arrangement and active site architecture. KAS I typically consists of multiple domains, including an *N*-terminal domain responsible for ACP binding and a C-terminal domain housing the catalytic active site. Understanding the structural details and dynamics of KAS I is essential for elucidating its enzymatic mechanism and for designing inhibitors that can selectively target bacterial fatty acid synthesis. Inhibition of KAS I activity can disrupt bacterial membrane integrity, leading to growth inhibition or cell death, making it an attractive target for the development of novel antibacterial agents. Docking studies utilizing the crystal structure of *E. coli* KAS I (1FJ4) can aid in the identification of potential inhibitors and provide insights into their binding modes and interactions, thereby facilitating the rational design of antibacterial compounds with improved efficacy and selectivity against bacterial pathogens such as *E. coli*.

The docking process had been done using MOE (Molecular Operating Environment). Firstly, the target protein structure (PDB ID: 1FJ4) is prepared by removing water molecules, adding hydrogen atoms, and assigning partial charges. The ligands, which are molecules to be docked into the protein, are also prepared by optimizing their geometry and generating 3D conformations. The protien active site is then selected using sitefinder in MOE tools. Docking calculations are then performed using MOE's docking algorithms. These algorithms systematically sample different orientations and conformations of the ligands within the binding site of the protein, evaluating their interactions and scoring the binding poses based on energy or scoring functions. The results of docking calculations are analyzed to identify the most favorable binding poses and interactions between the ligands and protein.

RESULTS AND DISCUSSION

Conductivity Measurement

The molar conductance of 1.0×10^{-3} mol dm^{-3} solution of all the complexes in DMSO were measured at room temperature. The molar conductance values (5 to 21 Ω^{-1} cm^2 mol^{-1}) indicated that all the complexes are non-electrolytic in nature[33,34] except Cr(III) complex which behaves as 1 : 1 electrolyte having molar conductance value 87 Ω^{-1} cm^2 mol^{-1}.[34]

Magnetic Moment and Electronic Spectral Studies

The observed values of effective magnetic moment (μ_{eff}) of the complexes at room temperature (29 °C) indicated that Cd(II) and Zn(II) complexes (μ_{eff} = 0.60–0.62 B.M) are diamagnetic whereas rest of the complexes (μ_{eff} = 1.74–5.96 B.M) are paramagnetic in nature.[35] The electronic spectra of the ligand and all the complexes were recorded within the UV-visible range (200–800 nm) at room temperature after dissolving into DMSO solvent. The electronic spectrum of the ligand showed absorption peaks at 275 nm and 340 nm which is attributed to the $\pi{\rightarrow}\pi^*$ and $n{\rightarrow}\pi^*$ transition respectively.[33,36–39] The UV–visible spectra of Cu(II), Co(II) and Zn(II) complexes showed the presence of three strong absorption bands. The Cu(II), Co(II) and Zn(II) complexes exhibited a peak at 287, 283 and 289 nm respectively may have attributed to $\pi{\rightarrow}\pi^*$ transition. Another peak at 357, 380 and 396 nm respectively may have assigned as $n{\rightarrow}\pi^*$ transition due to lone pair electrons of an azomethine nitrogen and an antibonding p orbital.[40–43] The presence of an absorption band at 271, 262 and 262 nm respectively presumably caused by charge transfer (CT) transition.[33,44] The electronic spectrum of Ni(II) complex showed bands at 257, 381 and 575 nm. The peak at 257 nm is due to charge transfer (CT) transition where peak at 381 and 575 nm may be assigned to $^3A_{2g}(F) \rightarrow {}^3T_{1g}(P)$ and $^3A_{2g}(F) \rightarrow {}^3T_{1g}(F)$ respectively.[42,43,45,46] The UV-visible spectrum of Cr(III) complex showed three bands at 256, 350 and 622 nm. The peak at 256 nm and 350 nm is due to CT and $n{\rightarrow}\pi^*$ transition respectively. A very weak peak at 622 nm may be assigned to $^6A_{1g} \rightarrow {}^4T_{1g}$.[47,48] Cd(II) complex showed only two absorption peaks at 274 nm and 339 nm which is attributed to the CT and $n{\rightarrow}\pi^*$ transition respectively. The Mn(II) complex exhibited four absorption peak at 261, 274, 344 a nd 646 nm. The peak at 261, 274 and 344 nm may have assigned as CT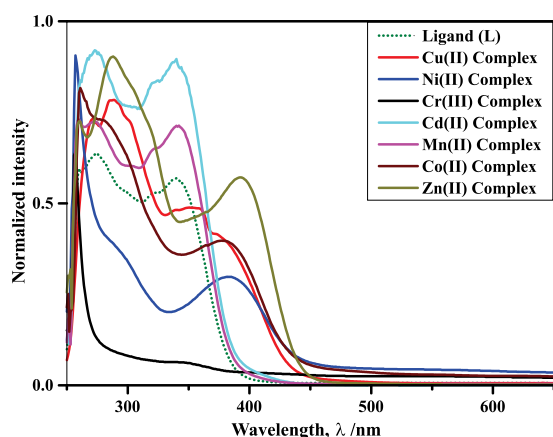, $\pi{\rightarrow}\pi^*$ and $n{\rightarrow}\pi^*$ transition respectively.[33,40,41,44] A very weak peak at 646 nm may be assigned to $^4T_{1g} \rightarrow {}^4T_{2g}$ (F) for Mn(II) complex.[44,45]

From the above explanation, the UV-visible absorption peak of the ligand at 275 nm and at 340 nm were shifted in all the complexes (Figure 1) indicating the coordination of the ligand to the metal ions through the nitrogen atom of the azomethine group. The electronic spectral data coupled with the magnetic moment value suggested that the Cu(II), Cd(II), Co(II) and Zn(II) complexes possess to have tetrahedral geometry where Ni(II), Cr(III) and Mn(II) complexes have octahedral geometry.

IR Spectral Studies

The IR spectrum of Schiff base ligand showed the presence of an absorption band at 1623 cm^{-1}, which is assigned as azomethine, v(C=N) linkage. The absence of bands at 1735 cm^{-1} for carbonyl v(C=O) and 3420 cm^{-1} for v(NH$_2$) stretching vibration indicating that aldehyde and amino moieties of the starting reagents had been converted into the azomethine moiety.[49,50] The infrared spectra of the ligand showed an absorption band at 3436 cm^{-1} due to the presence of v(−OH) stretching.[49,50] The strong band at 1157 cm^{-1} for v(C−O) indicated that C−O bond was present in the Schiff base ligand.[51–53] The IR spectra also showed clear v_{asy}(COO$^-$) and v_{sy}(COO$^-$) band at 1573 cm^{-1} and 1418 cm^{-1} respectively.[54]

On complexation of Schiff base with various metal ions, v(C=N) band was shifted to lower frequency (1620−1616 cm^{-1}) (Figure 2) due to the bonding between the donor nitrogen atom and the metal ion in the complexes.[49,50] Moreover, carboxylic and the phenolic v(OH) disappeared as the deprotonated oxygen atom of these groups act as donor atom to the metal ions.[54,55] New v(OH) vibrational frequencies at (3435−3401 cm^{-1}) due to the coordinated water molecule as also supported by thermal analysis.[54,46,57] The shifting of v_{asy}(COO$^-$) and v_{sy}(COO$^-$) band in lower frequencies in the range (1569−1544 cm^{-1}) and (1398−1384 cm^{-1}) respectively indicates the coordination through the oxygen of carboxyl group.[54] Shifting of v(C-O) band to the lower frequency (1156−1140 cm^{-1}) is also the indication of coordination through the phenolic oxygen.[51–53] In comparison of the spectra of Schiff base and its metal complexes suggested that the Schiff base coordinated to metal ions using three donors, indicated that the ligand acted as a tridentate ligand. Further conclusive evidence is the appearance of weak low frequency new absorption bands in the range 525−532 cm^{-1} and 385−447 cm^{-1} that assigned the metal-oxygen v(M-O) and metal–nitrogen v(M−N) frequency respectively.[33,47,51,58,59] The appearance of v(M−O) and v(M-N) vibrations support the involvement of N and O atoms in complexation with metal ions.

Figure 1. UV-Vis spectra of Schiff base ligand (L) and its metal complexes.
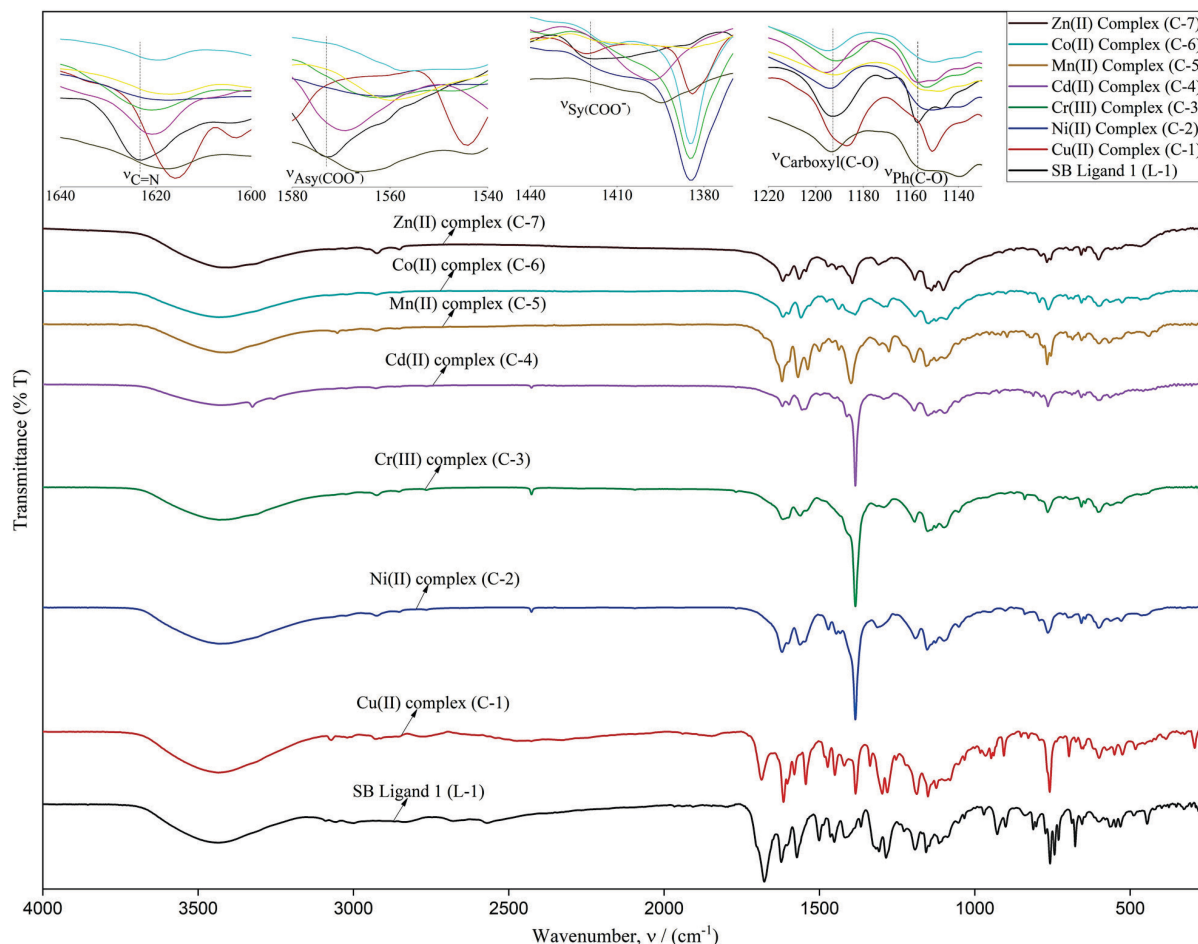
Figure 2. FTIR spectra of Schiff base ligand (L) and its metal complexes.

ESI-MS Spectra

ESI-MS can provide important information concerning the structure, stoichiometry, and metal oxidation state of dissolved metal complexes. The ESI-Mass spectra of the ligand and complexes are presented in Figure 3. The obtained *m / z* values are similar to the formula weight which further supports the proposed structure of the synthesized compounds.

Thermal Analysis (TGA/DTG)

The thermal analysis of solid Cu(II), Ni(II), Cd(II), Mn(II), Co(II) and Zn(II) metal complexes were carried out under nitrogen atmosphere and heating rate was suitably controlled at 30 °C min^{-1} and the weight loss was measured from the ambient temperature up to 800 °C. The TGA and DTG curve of the complexes (Figure 4) clearly indicated that the decomposition of the complexes proceeds in three or four steps. There were some minor steps and asymmetry of TGA/DTG curves also observed. The weight losses for each complex was calculated within the corresponding temperature ranges. The different thermodynamic parameters are listed in Table 1. The TGA and DTG curve of Cu(II), Ni(II) and Mn(II) complexes indicated that they decomposed into three main steps, while Cd(II), Co(II) and Zn(II) metal complexes were decomposed into four steps. In case of Co(II) complexes, the first step of decomposition (calculated 5.38 % and found 4.40 %) at temperature range 30–142 °C assigned to the loss of lattice water outside the coordination sphere.[33,42,43,50] In case of all other complexes at the range 57–390 °C the maximum weight losses are attributable to the loss of coordinated water.[42,46] In the temperature range of 272–560 °C, most of the part of the complexes have been degraded. Above 550–600 °C temperature, these complexes decomposed and removed as metal/metal oxide. Therefore, the thermal analysis of the synthesized complexes confirms the presence of lattice and coordinated water molecule and supports the proposed structure of the synthesized metal complexes. Possible thermal degradation pathway of the complexes has presented in Figure 5.
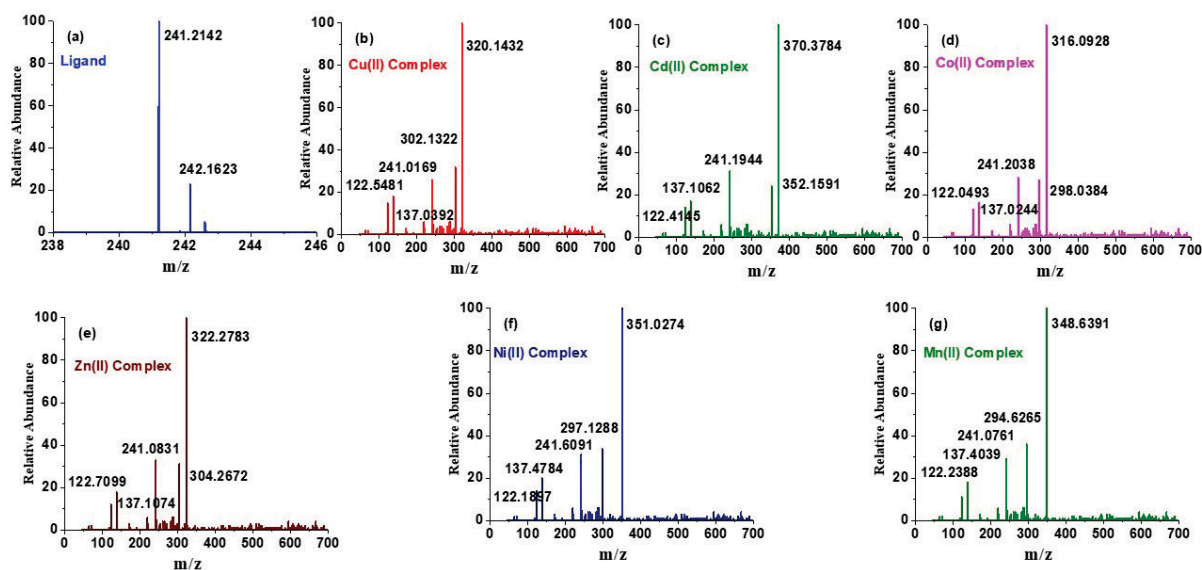
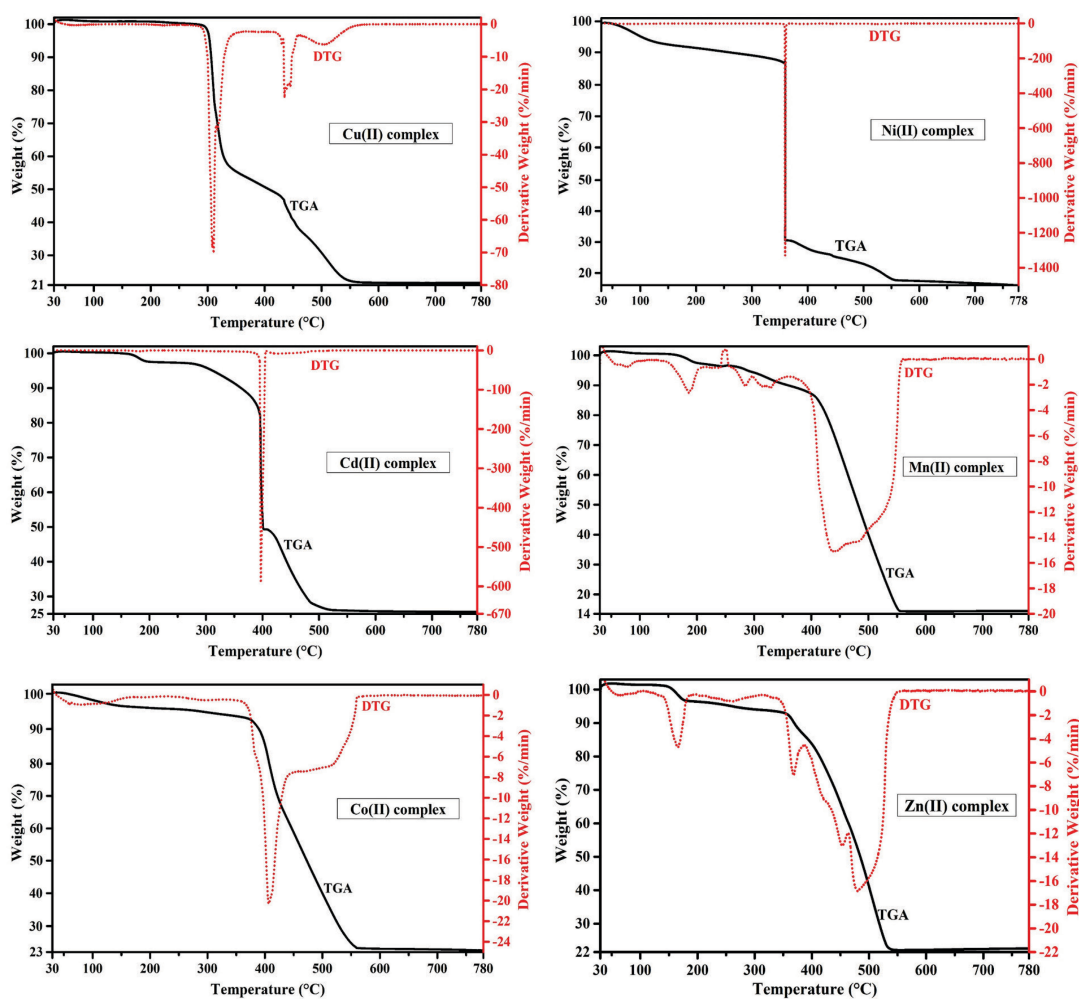**Figure 3.** ESI-MS spectra of the synthesized compounds.

Figure 4. TGA-DTG curve representing thermal degradation of the metal complexes.

Table 1. Thermal data of Cu(II), Ni(II), Cd(II), Mn(II), Co(II) and Zn(II) complexes.

Complexes	Steps	Temperature range/ °C	DTG peak/ °C	TG mass loss % calc./found	Assignments
$[Cu(C_{14}H_9NO_3)\cdot H_2O]$	1st	285–357	311	43.06 / 44.64	$C_7H_6O_3$
	2nd	360–560	435	37.13 / 35.01	$-NC_7H_5O-$
	3rd	>600		24.80 / 21.65	Cu / CuO
$[Ni(C_{14}H_9NO_3)(H_2O)_3]$	1st	57–350	–	15.38 / 14.50	$3H_2O$
	2nd	350–500	360	68.16 / 67.50	$C_{14}H_9NO_3$
	3rd	>550		16.72 / 18.00	Ni / NiO
$[Cd(C_{14}H_9NO_3)\cdot H_2O]$	1st	136–200	183	4.87 / 4.35	H_2O
	2nd	272–403	397	39.80 / 46.26	$C_8H_5NO_2$
	3rd	405–550		24.91 / 24.43	C_6H_4O
	4th	>600	–	30.29 / 25.57	Cd / CdO
$[Mn(C_{14}H_9NO_3)(H_2O)_3]$	1st	140–390	185	15.50 / 14.10	$3H_2O$
	2nd	400–560	440	68.70 / 71.66	$C_{14}H_9NO_3$
	3rd	>560		15.79 / 14.34	Mn / MnO
$[Co(C_{14}H_9NO_3)\cdot H_2O]\cdot H_2O$	1st	30–142	71	5.38 / 4.40	H_2O
	2nd	360–446	406	41.32 / 36.27	$C_7H_6O_3$
	3rd	450–560	503	35.62 / 36.00	$-NC_7H_5O-$
	4th	>600		22.44 / 23.33	Co / CoO
$[Zn(C_{14}H_9NO_3)\cdot H_2O]$	1st	139–194	169	5.59 / 4.80	H_2O
	2nd	300–455	369	37.19 / 36.66	$C_7H_4O_2$
	3rd	455–536	470	36.92 / 35.91	$-NC_7H_5O-$
	4th	>550		20.15 / 22.09	Zn / ZnO
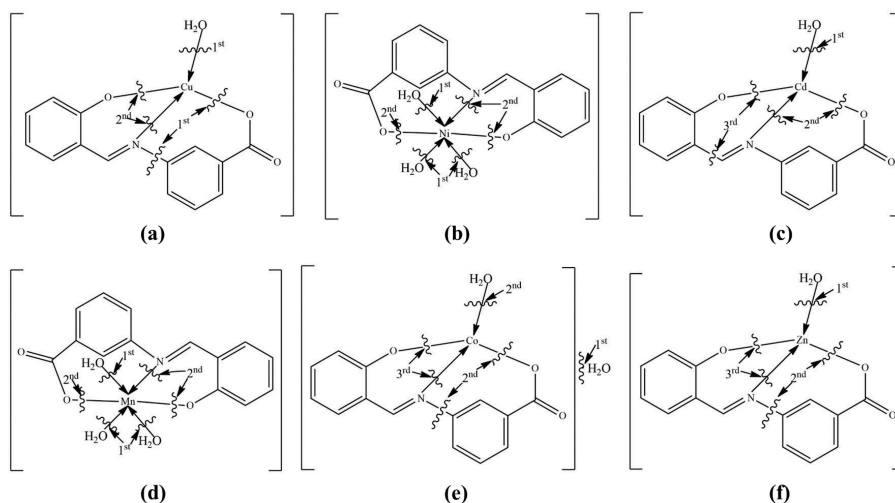
Figure 5. Possible thermal degradation pathway of the (a) Cu(II) (b) Ni(II) (c) Cd(II) (d) Mn(II) (e) Co(II) and (f) Zn(II) complexes.

DFT Calculations

The optimized structures of free ligand and its metal complexes were shown in Figure 6. Optimization of Cu(II), Cd(II), Co(II) and Zn(II) complexes gave four coordination geometry as $[M(L)(H_2O)]$, Figure 6. Take in consideration the bond angles; it is obvious that Cu(II), Cd(II), Co(II) and Zn(II) complexes formed distorted tetrahedral geometry. For further confirmation, the degree of distortion in a four coordinate geometry (τ_4) was calculated.[26] The degree of distortion, $\tau_4 = 1$ and 0 for perfect tetrahedral and square planar geometry, respectively. The Cu(II), Cd(II), Co(II) and Zn(II) complexes had $\tau_4 = 0.84$, 0.87, 0.88, and 0.86,

respectively, which was adopted with tetrahedral geometry. While, the optimization of Ni(II), Cr(III), and Mn(II) complexes gave octahedral geometry as $[M(L)(H_2O)_3]$, Figure 6.

The frontier molecular orbitals are the most important orbitals in a molecule.[60] Both the HOMO and LUMO orbitals play a role in chemical reactivity/stability.[61] The negative values of E_{HOMO} and E_{LUMO} indicate the molecule's stability. The higher HOMO energy suggested that the molecule is a good electron donor, and that this property is important for the creation of a charge-transfer complex between the molecule and the biological target. Low HOMO energy values, on the other hand, suggest that
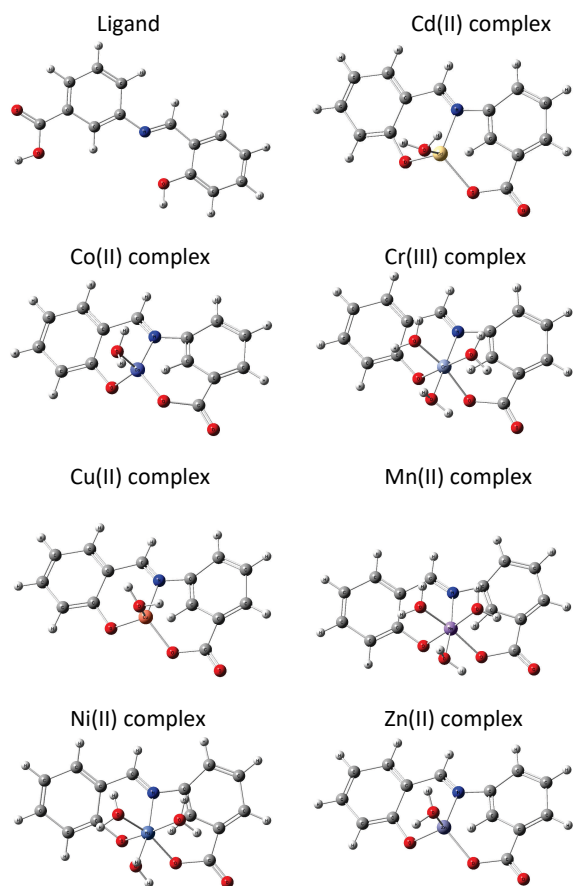
Figure 6. 3D optimized structure of the target compounds.

a molecule's ability to donate electrons is weaker, whereas LUMO energy indicates a molecule's ability to accept an electron.[62]

The DFT-calculated HOMO and LUMO energies of the studied compounds are listed in Table 2. In addition, Figure 7 depicts a graphical representation of their HOMO-LUMO distribution as well as their respective positive and negative regions. Green and red are used to indicate the positive and negative phases, respectively.

HOMO and LUMO, or frontier molecular orbitals, are crucial in many aspects of a chemical as well as quantum chemistry. The energy difference between the HOMO and the LUMO is crucial in influencing a molecule's electrical characteristics, kinetic stability, optical polarizability, and chemical reactivity descriptors like hardness and softness. The concept of hardness and softness is related to a compound's reactivity and is a quality that quantifies how much chemical reactivity can be stabilized by adding a charge.[63]

A high gap denotes a hard molecule, which is associated with more stable molecules, and a small gap denotes a soft molecule, which is associated with more reactive molecules. Also, smaller indicates simpler charge
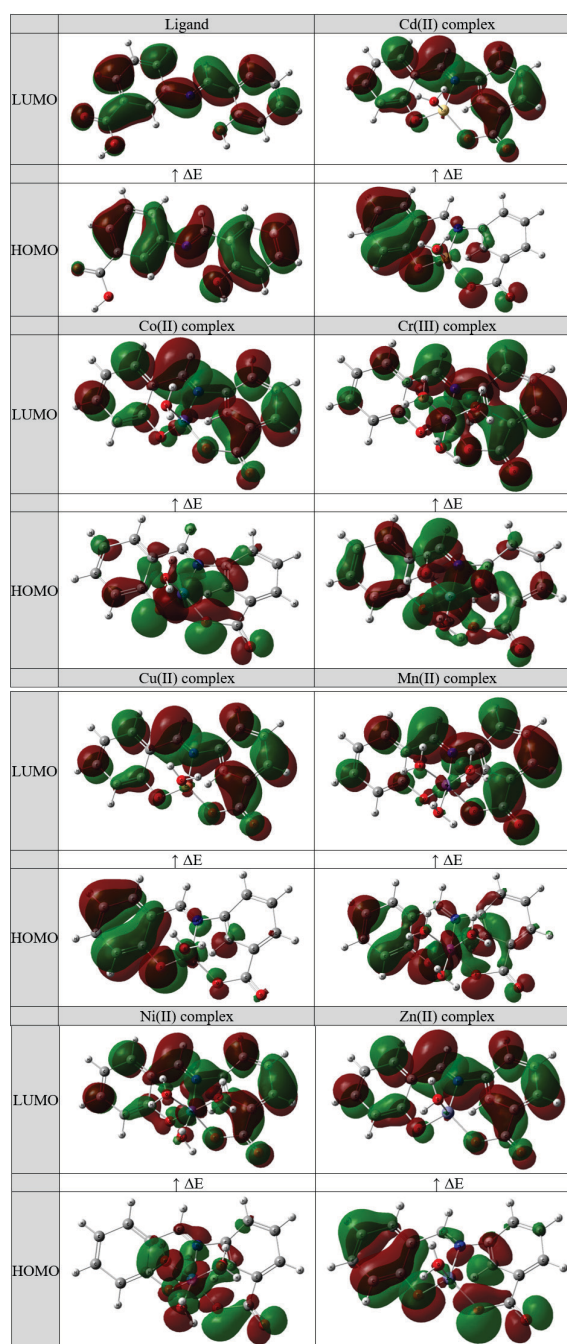
Figure 7. Graphical representation of HOMO-LUMO distribution.

transfer and polarization inside the molecule, which is linked to strong chemical reactivity, low kinetic stability, and effective electronic charge transfer interactions, making the molecule highly polarizable.[64,65] According to ΔE, the reactivity trend was in the following order: Cr(III) complex > Ni(II) complex > Co(II) complex > Cu(II) complex > Mn(II) complex > Cd(II) complex > Zn(II) complex > Ligand, Table 2.

Table 2. Quantum chemical descriptors.

	HOMO	LUMO	ΔE	I	A	η	σ
Ligand	−6.25	−2.05	4.20	6.25	2.05	2.10	0.24
Cd(II) complex	−5.81	−2.64	3.17	5.81	2.64	1.59	0.32
Co(II) complex	−5.51	−2.79	2.72	5.51	2.79	1.36	0.37
Cr(III) complex	−3.89	−2.43	1.46	3.89	2.43	0.73	0.69
Cu(II) complex	−5.74	−2.80	2.94	5.74	2.80	1.47	0.34
Mn(II) complex	−5.34	−2.30	3.04	5.34	2.30	1.52	0.33
Ni(II) complex	−4.17	−2.69	1.48	4.17	2.69	0.74	0.67
Zn(II) complex	−5.87	−2.63	3.25	5.87	2.63	1.62	0.31

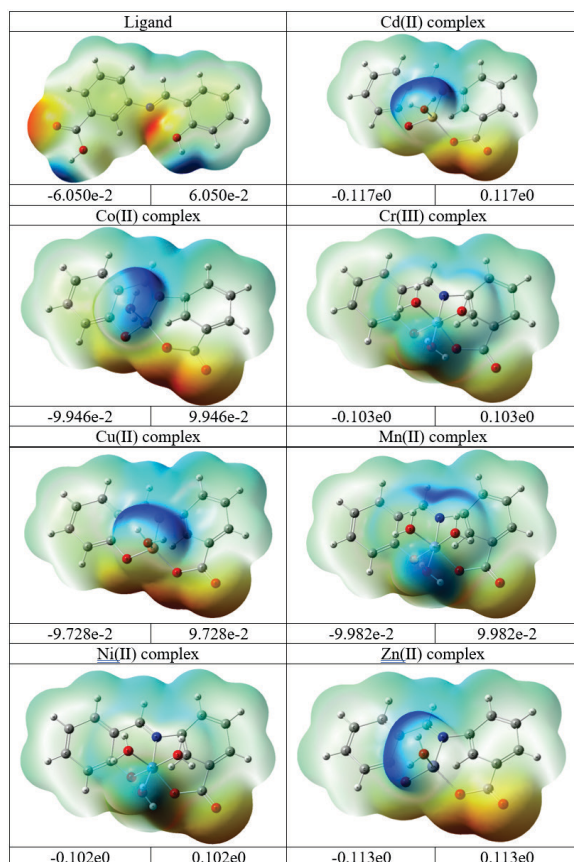The protein and substrate both have partial charges, and these charges play a critical role in determining how successfully the substrate and protein will bind together. Through the use of the molecular electrostatic potential (MEP) diagram, the topological and structural properties of three-dimensional substrates can be learned about. Where the nuclei or electrons have the most influence on the molecular geometry is determined by the Molecular Electrostatic Potential (MEP).[66,67]

A MEP diagram uses a gradient of colors, from blue to red, to visually indicate the range of values contained in the diagram. There is a connection between the positively charged (blue) and negatively charged (red) areas of the MEP, which, respectively, are in charge of electrophilic and nucleophilic reactivity. The negative charge that is present on the surface is reflected by the red hues (i.e., those parts where accepting an electrophile is most promising). When the negative charge of a molecule increases, it indicates that the critical sites on that compound are getting more attracted to electrophiles as reactions progress.

The molecular electrostatic potential (MEP) diagram is shown in Figure 8. The majority of the negative sites, shown by the color red, can be seen grouped around the oxygen and nitrogen moieties in the substrates of interest. This oxygen and nitrogen moieties is itself surrounded by a large number of electrons, making it an appealing target for electrophilic attack. The coordinated hydrogen moiety, which may operate as an H-bond donor in protein-substrate intermolecular interactions, is primarily targeted by the more positive regions (blue) Figure 8.

Figure 8. MEP diagram of the target compounds.

Molecular Docking

To validate the experimental biological activity, the molecular docking approach was studied to give a more scientific way of justification to the drug action of target compounds. The molecular docking was implemented to evaluate the behavior at biological interfaces by choosing *E. coli* (KAS I-PDB ID-1FJ4) receptor from RCSB Protein Data Bank. The scores due to docking for the tested substrates determined that all the prepared compounds possessed potential for interaction with one or more amino acids in the active site (binding pocket) of the receptor. The Cu(II), Cd(II) and Zn(II) complexes were the most potent inhibitors of the receptor. In the docking, the binding of Cu(II), Cd(II) and Zn(II) complexes were supported by strong interactions with possible amino acid residues, Table 3. The Cd(II) complex, contributed the highest docking score −7.18 kcal mol⁻¹, then Zn(II) complex with docking score −7.06 kcal mol⁻¹, and finally the

Md. N.A. BITU et al.: Metal Complexes of the Schiff Base ...

(not final pg. №) **11**

	3D	2D	3D	2D

Ligand

Cd(II) complex

Co(II) complex

Cr(III) complex

Cu(II) complex

Mn(II) complex

Ni(II) complex

Zn(II) complex

Figure 9. Docking interactions.

Cu(II) complex with docking score −6.86 kcal mol⁻¹, compared to the other remaining compounds. The binding site of the current compounds in the active site of 1FJ4 interaction 2D and 3D were represented in Fig. 9 and the docking data was tabulated in Table 3. The Cd(II) complex form one hydrogen bond donor between O29 with Thr300, and one hydrogen bond acceptor between O18 with Thr302, in addition to one pi-pi interaction between 6-ring with Phe390, with average distance of 2.74, 3.31, and 3.07 Å, respectively. The Zn(II) complex form one hydrogen bond donor between C5 with Glu309, and two hydrogen bond acceptor between O18 with Cys163, and His333, with average distance of 2.91, 3.12, and 3.06 Å, respectively. The Cu(II) complex form two hydrogen bond donor between

Table 3. Docking data.

	Ligand	Receptor	Interaction	Distance	E / kcal mol^{-1}	S / kcal mol^{-1}
	O 18	HIS 298	H-acceptor	2.97	−1.80	
Ligand	O 18	GLY 391	H-acceptor	3.74	−0.60	−5.34
	6-ring	PHE 390	pi-pi	3.64	−0.38	
	O 29	GLY 391	H-donor	2.74	−4.40	
Cd(II) complex	O 18	GLY 391	H-acceptor	3.31	−0.80	−7.18
	6-ring	PHE 390	pi-pi	3.07	−0.22	
	O 29	THR 300	H-donor	2.92	−5.90	
Co(II) complex	O 18	THR 302	H-acceptor	3.09	−1.20	−5.35
	6-ring	PHE 390	pi-pi	3.77	−0.31	
	C 5	GLU 309	H-donor	2.91	−0.80	
	C 6	ASP 306	H-donor	3.28	−0.80	
Cr(III) complex	O 32	THR 300	H-donor	2.76	−0.80	−5.41
	O 18	CYS 163	H-acceptor	3.54	−0.70	
	O 18	GLY 391	H-acceptor	3.32	−0.80	
	O 29	ASP 265	H-donor	2.73	−3.30	
Cu(II) complex	O 29	ASN 396	H-donor	2.72	−3.60	−6.86
	O 29	ASP 265	ionic	3.56	−1.70	
	6-ring	PHE 390	pi-pi	3.90	−0.43	
	O 32	VAL 270	H-donor	2.47	−2.50	
Mn(II) complex	O 33	THR 302	H-donor	2.75	−3.60	−5.29
	6-ring	THR 300	pi-H	3.80	−0.70	
	O 33	THR 302	H-donor	2.81	−3.90	
Ni(II) complex	O 18	HIS 298	H-acceptor	2.80	−1.30	−5.32
	O 18	HIS 333	H-acceptor	3.75	−0.50	
	C 5	GLU 309	H-donor	2.91	−0.80	
Zn(II) complex	O 18	CYS 163	H-acceptor	3.12	−0.80	−7.06
	O 18	HIS 333	H-acceptor	3.06	−3.10	

O29 with Asp265 and Asn396, and one ionic interaction between O29 with Asp265, in addition to one pi-pi interaction between 6-ring with Phe390, with average distance of 2.73, 2.72, 3.56 and 3.90 Å, respectively.

Antibacterial Activity

The principal objective of performing the antibacterial screening is to determine the susceptibility of the pathogenic microorganism to the synthesized compounds. The free Schiff base ligand and their metal complexes screened for their antibacterial activity against two pathogenic bacterial strains, the *Bacillus cereus* ATCC 25923 and *Escherichia coli* ATCC 25922 with Kanamycin (K-30) standard. The compounds were tested at a
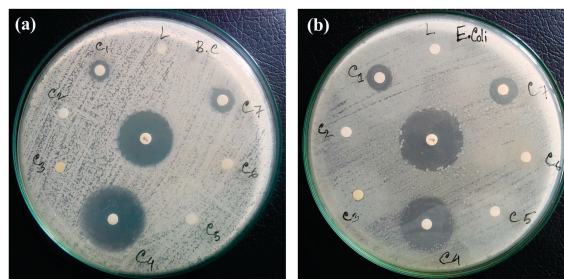

Figure 10. Photographic representation of zone of inhibition of Schiff base ligand and its metal complexes against (a) *Bacillus cereus* ATCC 25923 and (b) *Escherichia coli* ATCC 25922.
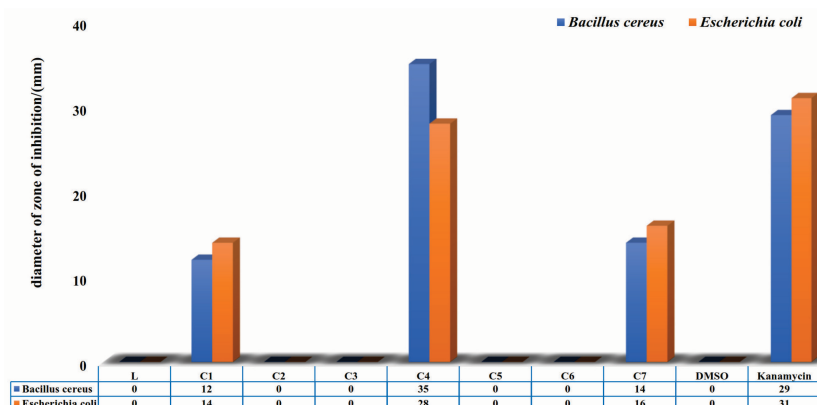
Figure 11. Graphical representation of antibacterial activity of synthesized ligand and its complexes with *Kanamycin 30* standard against *Bacillus cereus* and *Escherichia coli*.

concentration of 50 μg / 10 μL (i.e. 50 μg / disc) in DMSO solution using investigated by using the traditional disc diffusion method.[68–73] The inhibitory zones measured in diameter (mm) were the clear zones around the discs killing the pathogens Figure 10. The result of screening of the Schiff base and all the metal complexes exhibited varying degrees of antibacterial activity against both the tested bacterial species Figure 11. Among all the synthesized species Cu(II), Cd(II) and Zn(II) complexes possess to have potential activity than the others towards the tested pathogens.

Cytotoxic Activity

The cytotoxic activity of Cu(II), Cd(II) and Zn(II) complexes was examined on human umbilical vein endothelial cells (HUVECs). The cells grown on Dulbecco's modified Eagle medium (DMEM). HUVECs were plated at density of 6000 cells per well in a 96-well cell culture plate and allowed to grow in a humidified 5 % CO_2 incubator at 37 °C for 24 h. Cells were treated with 5 μg mL^{-1}, 10 μg mL^{-1} and

20 μg mL^{-1} of each complexes for 48 h. Cell viability was obtained by colorimetric method. A publicly accessible IC$_{50}$ calculator online tool from AAT Bioquest (https://www.aatbio.com/tools/ic50-calculator) used to find the IC$_{50}$ values.[74] The toxicities of 20 μg mL^{-1} of Cu(II), Cd(II) and Zn(II) complexes are found to be 39.33 %, 31.43 %, and 27.73 %, respectively Table 4. According to these results, Cu(II) complex is found to behave as a better antitumor agent on HUVECs. The percentage of cell viability versus different concentrations of the complexes for human umbilical vein endothelial cells shown in Figure 12. The IC$_{50}$ values obtained in this study, shown in Table 5. The IC$_{50}$ value of the Zn(II) complex (11 ± 0.18 μg mL^{-1}) is higher than the Cu(II) complex (10 ± 0.31 μg mL^{-1}) and Cd(II) complex (11 ± 0.02 μg mL^{-1}).

Table 4. In vitro cytotoxicity of the complexes for HUVECs.

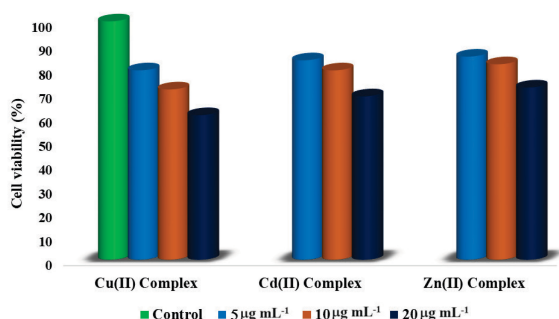| Concentration / μg mL^{-1}	Absorbance	Toxicities / %	Cell viability / %
Control	0.2266	0	100
Cu(II) complex			
5	0.1027	20.53	79.47
10	0.0813	28.54	71.46
20	0.0786	39.33	60.67
Cd(II) complex			
5	0.0871	16.32	83.68
10	0.0780	20.54	79.46
20	0.0723	31.43	68.57
Zn(II) complex			
5	0.0802	14.78	85.22
10	0.0766	17.98	82.02
20	0.0626	27.73	72.27

Figure 12. Percentage of cell viability for HUVECs exposed to the metal complexes of different concentrations after 48h incubation.

Table 5. IC$_{50}$ range of complexes for HUVECs.

Name of the Compound	IC$_{50}$ / µg mL^{-1}
Cu(II) Complex	10 ± 0.31
Cd(II) Complex	11 ± 0.02
Zn(II) Complex	11 ± 0.18

CONCLUSIONS

In this research paper, we have mentioned the synthesis of a Schiff base from the condensation of 3-amino benzoic acid with salicylaldehyde. The coordination chemistry of the synthesized amino acid derived Schiff base [3-((2-hydroxybenzylidene)amino)benzoic acid], [C$_{14}$H$_{11}$NO$_3$] and its Cu(II), Ni(II), Cr(III), Cd(II), Mn(II), Co(II) and Zn(II) complexes have also explored. The FTIR Spectral evidence indicated that the Schiff base behaved as N, O donor tridentate ligand. Magnetic moment value coupled with electronic spectral data suggested that Cu(II), Cd(II), Co(II) and Zn(II) complexes have tetrahedral geometry while Ni(II), Cr(III), and Mn(II) complexes have octahedral geometry which is further supported by the thermogravimetric analysis, ESI-MS spectra and also DFT calculations. TGA/DTG data showed the possible degradation pathway of the complexes and indicated that the complexes were thermally stable up to (200–300) °C. The molar conductance values indicated all the complexes to be non-electrolytic in nature except Cr(III) complex which behaves as 1 : 1 electrolyte. The Schiff base and its metal complexes have been screened for their antibacterial activity against *Bacillus cereus* and *Escherichia coli*. Among all the synthesized species Cu(II), Cd(II) and Zn(II) complexes were more potential towards the tested pathogens. The cytotoxic activity of Cu(II), Cd(II) and Zn(II) complexes was examined on human umbilical vein endothelial cells (HUVECs). Among these complexes, Cu(II) complex is found to show higher toxicities than the others on HUVECs.

REFERENCES

[1]   M. N. A. Bitu, M. S. Hossain, A. A. S. M. Zahid, C. M. Zakaria, M. Kudrat-E-Zahan, *Am. J. Heterocycl. Chem.* **2019**, *5*, 11–23.

[2]   M. Boybay, M. Sekerci, *Russ. J. Gen. Chem.* **2002**, *72*, 1266–1270.
https://doi.org/10.1023/A:1020844216503

[3]   M. Azam, M. N. A. Bitu, R. K. Mohapatra, S. I. Al-Resayes, L. Pintilie, S. M. Wabaidur, F. F. Alqahtani, M. S. Islam, A. K. Sarangi, M. Kudrat-E-Zahan, *J. Saudi Chem. Soc.* **2021**, *25*, 101207.
https://doi.org/10.1016/j.jscs.2021.101207

[4]   M. Emayavaramban, K. Kumar, P. Mani, B. Prabhakaran, A. Muthuvel, *Int. J. Adv. Chem.* **2014**, *2*, 20–23.
https://doi.org/10.14419/ijac.v2i1.1628

[5]   M. F. A. Ahmed, V. M. Yunus, *Orient. J. Chem.* **2014**, *30*, 111–117.
https://doi.org/10.1016/j.jocn.2014.06.044

[6]   G. Kumari, D. Kumar, C. P. Singh, A. Kumar, V. B. Rana, *J. Serb. Chem. Soc.* **2010**, *75*, 629–637.
https://doi.org/10.2298/JSC090704037K

[7]   S. M. Sondhi, N. Singh, A. Kumar, O. Lozach, L. Meijer, *Bioorg. Med. Chem.* **2006**, *14*, 3758–3765.
https://doi.org/10.1016/j.bmc.2006.01.054

[8]   K. N. Venugopala, B. S. Jayashree, *Indian J. Heterocycl. Chem.* **2003**, *12*, 307–310.

[9]   A. Pandey, R. Rajavel, S. Chandraker, D. Dash, *J. Chem.* **2012**, *9*, 2524–2531.
https://doi.org/10.1155/2012/145028

[10] R. P. Chinnasamy, R. Sundararajan, S. Govindaraj, *J. adv. pharm. technol res.* **2010**, *1*, 342–347.
https://doi.org/10.4103/0110-5558.72428

[11] T. Aboul-Fadl, F. A. Mohammed, E. A. Hassan, *Arch. Pharm. Res.* **2003**, *26*, 778–784.
https://doi.org/10.1007/BF02980020

[12] R. Miri, N. Razzaghi-asl, M. K. Mohammadi, *J. Mol. Model.* **2013**, *19*, 727–735.
https://doi.org/10.1007/s00894-012-1586-x

[13] P. G. Avaji, C. H. Vinod Kumar, S. A. Patil, K. N. Shivananda, C. Nagaraju, *Eur. J. Med. Chem.* **2009**, *44*, 3552–3559.
https://doi.org/10.1016/j.ejmech.2009.03.032

[14] W. A. Zoubi, A. A. S. Al-Hamdani, M. Kaseem, *Appl. Organomet. Chem.* **2016**, *30*, 810–817.
https://doi.org/10.1002/aoc.3506

[15] M. Bingöl, N. Turan, *J. Mol. Struct.* **2020**, *1205*, 127543.
https://doi.org/10.1016/j.molstruc.2019.127542

[16] Z. H. Chohan, M. Arif, M. Sarfraz, *Appl. Organomet. Chem.* **2007**, *21*, 294–302.
https://doi.org/10.1002/aoc.1200

[17] M. Pervaiz, M. Yousaf, I. Ahmad, A. Munawar, Z. Saeed, A. Adnan, T. Gulzar, S. Kirn, T. Kamal, A. Ahmad, *Spectrochim. Acta - A: Mol. Biomol. Spectrosc.* **2019**, *206*, 642–649.
https://doi.org/10.1016/j.saa.2018.05.057

[18]   M. Shebl, *J. Coord. Chem*. **2009**, *62*, 3217–3231. https://doi.org/10.1080/00958970903012785

[19]   H. M. A. Sharif, D. Ahmed, H. Mir, *Pak. J. Pharm. Sci*. **2015**, *28*, 449–455.

[20]   Y. Bayeh, F. Mohammed, M. Gebrezgiabher, F. Elemo, M. Getachew, M. Thomas, *Adv. Biol. Chem*. **2020**, *10*, 127–139. https://doi.org/10.4236/abc.2020.105010

[21]   A. Blagus, D. Cinčić, T. Friščić, B. Kaitner, V. Stilinović, *Maced. J. Chem. Chem. Eng*. **2010**, *29*, 117–138. https://doi.org/10.20450/mjcce.2010.159

[22]   M. I. Ali, S. Helen, M. Das, M. R. Juwel, M. A. K. Liton, *Mol. Phys*. **2023**, *121*, e2152745. https://doi.org/10.1080/00268976.2022.2152745

[23]   A. D. Becke, *Phys. Rev. A*. **1998**, *38*, 3098–3100. https://doi.org/10.1103/PhysRevA.38.3098

[24]   C. Lee, W. Yang, R. G. Parr, *Phys. Rev. B*. **1988**, *37*, 785-789. https://doi.org/10.1103/PhysRevB.37.785

[25]   A. D. Becke, *J. Chem. Phys*. **1993**, *98*, 5648–5652. https://doi.org/10.1063/1.464913

[26]   A. D. McLean, G. S. Chandler, *J. Chem. Phys*. **1980**, *72*, 5639–5648. https://doi.org/10.1063/1.438980

[27]   K. Raghavachari, J. S. Binkley, R. Seeger, J. A. Pople, , *J. Chem. Phys*. **1980**, *72*, 650–654. https://doi.org/10.1063/1.438955

[28]   P. J. Hay, W. R. Wadt, *J. Chem. Phys*. **1985**, *82*, 270–283. https://doi.org/10.1063/1.448799

[29]   W. R. Wadt, P.J. Hay, *J. Chem. Phys*. **1985**, *82*, 284–298. https://doi.org/10.1063/1.448800

[30]   E. K. Shokr, M. S. Kamel, H. Abdel-Ghany, M. A. E. A. A. Ali El-Remaily, A. Abdou, *Mater. Chem. Phys*. **2022**, *290*, 126646. https://doi.org/10.1016/j.matchemphys.2022.126646

[31]   N. A. A. Elkanzi, A. M. Ali, M. Albqmi, A. Abdou, *Appl. Organomet. Chem*, **2022**, *36*, e6868. https://doi.org/10.1002/aoc.6868

[32]   N. S. Abdel-Kader, H. Moustafa, A. L. El-Ansary, A. M. Farghaly, *Appl. Organomet. Chem*. **2022**, *36*, e6840. https://doi.org/10.1002/aoc.6840

[33]   M. S. Hossain, C. M. Zakaria, M. Kudrat-E-Zahan, *J. Sci. Res*. **2017**, *9*, 209–218. https://doi.org/10.3329/jsr.v9i2.29780

[34]   W. A. Zoubi, A. A. S. Al-Hamdani, S. D. Ahmed, Y. G. Ko, *J. Phys. Org. Chem*. **2017**, *31*, e3752. https://doi.org/10.1002/poc.3752

[35]   L. Mitu, A. Kriza,, *Asian J. Chem*. **2007**, *19*, 658–664. https://doi.org/10.1016/j.coi.2007.08.005

[36]   R. Islam, E. Uddin, N. A. Bitu, A. Asraf, F. Hossen, M. Haque, A. Mannan, Kudrat-E-Zahan, *Asian J. Res. Chem*. **2020**, *13*, 395–406. https://doi.org/10.5958/0974-4150.2020.00073.5

[37]   R. K. Al-Shemary, A. T. Numan, E. M. Atiyah, *Eur. Chem. Bull*. **2016**, *5*, 335–338.

[38]   N. K. Gondia, J. Priya, S. K. Sharma, *Res. Chem. Intermed*. **2017**, *43*, 1165–1178. https://doi.org/10.1007/s11164-016-2690-9

[39]   L. H. A. Rahman, A. M. Abu-Dief, N. A. Hashem, A. A. Seleem, *Int. J. Nano. Chem*. **2015**, *1*, 79–95.

[40]   K. Quari, S. Bendia, J. Weiss, C. Bailly, *Spectrochim. Acta - A: Mol. Biomol. Spectrosc*. **2015**, *135*, 624–631. https://doi.org/10.1016/j.saa.2014.07.034

[41]   J. R. Anacona, J. Calvo, O. A. Almanza, *Int. J. Inorg. Chem*. **2013**, 108740. https://doi.org/10.1155/2013/108740

[42]   M. S. Hossain, A. S. M. E. Shaheed, M. N. Khan, M. A. Mannan, M. M. Haque, C. M. Zakaria, R. K. Mohapartra, M. Kudrat-E-Zahan, *J. Chem. Bio. Phys. Sci*. **2018**, *8*, 654–668.

[43]   M. S. A. Dalia, F. Afsan, M. S. Hossain, M. A. Mannan, M. M. Haque, M. Kudrat-E-Zahan, *Asian J. Chem. Sci*. **2018**, *4*, JOCS.42355. https://doi.org/10.9734/AJOCS/2018/42355

[44]   M. Kudrat-E-Zahan, M. S. Islam, *Russ. J. Gen. Chem*. **2015**, *85*, 979–983. https://doi.org/10.1134/S1070363215040350

[45]   A. B. P. Lever, *Inorganic electronic spectroscopy*, 2nd edition, Elsevier, Amsterdam, **1984**.

[46]   F. Afsan, S. A. Dalia, S. Hossain, S. Sarker, Kudrat-E-Zahan, *Asian J. Chem*. Sci. **2018**, *4*, AJOCS.40913. https://doi.org/10.9734/AJOCS/2018/40913

[47]   M. S. Hossain, S. Sarker, A. S. M. Elias Shaheed, M. M. Hossain, A. A. Al-Bari, M. R. Karim, C. M. Zakaria, M. Kudrat-E-Zahan, *Chem. Biomol. Eng*. **2017**, *2*, 41–50.

[48]   M. S. Refat, H. K. Ibrahim, S. Z. A. Sowellim, M. H. Soliman, E. M. Saeed, *J. Inorg. Organomet. Polym. Mater*. **2009**, *19*, 521–531. https://doi.org/10.1007/s10904-009-9296-2

[49]   M. S. Hossain, C. M. Zakaria, M. Kudrat-E-Zahan, B. Zaman, *Der. Chem. Sin*. **2017**, *8*, 380–392.

[50]   M. S. Hossain, M. A. Islam, C. M. Zakaria, M. M. Haque, M. A. Mannan, M. Kudrat-E-Zahan, *J. Chem. Bio. Phys. Sci. Section A*, **2016**, *7*, 041–052.

[51]   N. Ljubijankić, V. Tešević, S. Grgurić-Šipka, M. Jadranin, S. Begić, L. Buljubašić, E. Markotić, S. Ljubijankić, *Bull. Chem. Tech. Bosnia and Herzegovina* **2016**, *46*, 1–6.

[52]   S. H. Baiu, M. M. El-Ajaily, N. M. El-Barasi, *Asian J. Chem*. **2009**, *21*, 5–10.

[53]   E. Pahontu, V. Fala, A. Gulea, D. Poirier, V. Tapcov, T. Rosu, *Molecules* **2013**, *18*, 8812–8836. https://doi.org/10.3390/molecules18088812

[54]   B. K. Al-Salami, A. H. Mohammed, K. A. Askar, *Res. J. Pharm. Biol. Chem. Sci*. **2014**, *5*, 1457–1474.

[55]   J. M. Gichumbi, H. B. Friedrich, B. Omondi, J. *Mol. Catal. A Chem*. **2016**, *416*, 29–38. https://doi.org/10.1016/j.molcata.2016.02.012

[56] N. Turan, K. Buldurun, *Eur. J. Chem*. **2018**, *9*, 22–29. https://doi.org/10.5155/eurjchem.9.1.22-29.1671

[57] M. Sebastian, V. Arun, P. P. Robinson, A. A. Varghese, R. Abraham, E. Suresh, K. K. M. Yusuf, *Polyhedron* **2010**, *29*, 3014–3020. https://doi.org/10.1016/j.poly.2010.08.016

[58] J. A. Shampa, M. R. Islam, M. S. Hossain, G. T. Rahman, C. M. Zakaria, M. Kudrat-E-Zahan, *Am. J. heterocycl. chem.* **2017**, *3*, 37–41. https://doi.org/10.11648/j.ajhc.20170304.11

[59] R. M. El-Bahnasawy, L. M. S. El-Deen, A. S. El-Table, M. A. Wahba, F. A. El-Monse, *Eur. Chem. Bull.* **2014**, *3*, 441–446.

[60] A. A. Nadia Elkanzi, H. Hrichi, H. Salah, M. Albqmi, A. M. Ali, A. Abdou, *Polyhedron* **2023**, *230*, 116219. https://doi.org/10.1016/j.poly.2022.116219

[61] Y. A. A. Alghuwainem, H. M. Abd El-Lateef, M. M. Khalaf, A. A. Abdelhamid, A. Alfarsi, M. Gouda, M. Abdelbaset, A. Abdou, *J. Mol. Liq.* **2023**, *369*, 120936. https://doi.org/10.1016/j.molliq.2022.120936

[62] Y. A. A. Alghuwainem, H. M. Abd El-Lateef, M. M. Khalaf, A. A. Amer, A. A. Abdelhamid, A. A. Alzharani, A. Alfarsi, S. S. Mohamed Gouda, A. Abdou, *Int. J. Mol. Sci.* **2022**, *23*, 15614. https://doi.org/10.3390/ijms232415614

[63] M. A. Arafath, F. Adam, M. B. K. Ahamed, M. R. Karim, M. N. Uddin, B. M. Yamin, A. Abdou, *J. Mol. Struct.* **2023**, *1278*, 134887. https://doi.org/10.1016/j.molstruc.2022.134887

[64] M. A. Latif, T. Ahmed, M. S. Hossain, B. M. Chaki, A. Abdou, M. Kudrat-E-Zahan, *Russ. J. Gen. Chem.* **2023**, *93*, 389–397. https://doi.org/10.1134/S1070363223020214

[65] M. A. Ibrahim Al-Gaber, H. M. Abd El-Lateef, M. M. Khalaf, S. Shaaban, M. Shawky, G.G. Mohamed, A. Abdou, M. Gouda, A. M. Abu-Dief, *Materials* **2023**, *16*, 897. https://doi.org/10.3390/ma16030897

[66] E. K. Shokr, M. S. Kamel, H. Abdel-Ghany, M. A. E. A. A. Ali El- Remaily, A. Abdou, *Mater. Chem. Phys*. **2022**, *290*, 126646. https://doi.org/10.1016/j.matchemphys.2022.126646

[67] N. A. A. Elkanzi, A. M. Ali, M. Albqmi, A. Abdou, *Appl. Organomet. Chem.* **2022**, *36*, e6868. https://doi.org/10.1002/aoc.6868

[68] M. M. Haque, M. Kudrat-E-Zahan, L. A. Banu, M. Shariful Islam, M. S. Islam, *Bioinorg. Chem. Appl.* **2015**, 923087. https://doi.org/10.1155/2015/923087

[69] L. A. Banu, M. S. Islam, M. A. Alim Al-Bari, M. Kudrat-E-Zahan, *Int. J. Rec. Adv. Multidiscip. Res*. **2015**, *2*, 0145–0148.

[70] M. Shiraj-U-Ddaula, M. A. Islam, S. Aktar, M. K. Islam, M. A. Alim Al-Bari, M. M. Haque, M. Kudrat-E-Zahan, *Asian J. Res. Chem.* **2014**, *7*, 619–621.

[71] M. M. Ali, M. N. A. Bitu, M. S. Hossain, M. F. Hossen, M. A. Asraf, M. A. Farooque, M. Kudrat-E-Zahan, *Asian J. Chem. Sci.* **2020**, *8*, 15–21. https://doi.org/10.9734/ajocs/2020/v8i119032

[72] M. A. Latif, T. Tofaz, B. M. Chaki, H. M. T. Islam, M. S. Hossain, M. Kudrat-E-Zahan, *Russ. J. Gen. Chem*. **2019**, *89*, 1197–1201. https://doi.org/10.1134/S107036321906015X

[73] V. Govindaraj, S. Ramanathan, S. Murgased, *Der. Chem. Sin.* **2018**, *9*, 736–745.

[74] M. Azam, S. M. Wabaidur, M. Alam, Z. Khan, I. O. Alanazi, S. I. Al-Resayes, Il. Soo Moon, Rajendra, *Transit. Met. Chem.* **2021**, *46*, 65–71. https://doi.org/10.1007/s11243-020-00422-8